Spatio-temporal characteristics of ion velocity in a Hall thruster discharge

2010 Plasma Sources Sci. Technol. 19 065018

(http://iopscience.iop.org/0963-0252/19/6/065018)

Plasma Sources Sci. Technol. **19** (2010) 065018 (9pp) doi:10.1088/0963-0252/19/6/065018

Spatio-temporal characteristics of ion velocity in a Hall thruster discharge

S Mazouffre and G Bourgeois

ICARE, CNRS, 1C avenue de la Recherche Scientifique, 45071 Orléans, France

E-mail: stephane.mazouffre@cnrs-oleans.fr

Received 28 June 2010, in final form 10 September 2010
Published 23 November 2010
Online at stacks.iop.org/PSST/19/065018

Abstract

The time evolution of the axial velocity of a metastable Xe^+ ion was examined in the crossed-field discharge of a PPS100-ML Hall thruster fired at 250 V by means of laser-induced fluorescence spectroscopy at 834.72 nm. A pulse-counting detection technique was employed to achieve a time resolution of 0.1 μs. A periodic break of 10 μs duration of the anode current is used to stabilize the discharge and allow the investigation of both forced and natural plasma oscillations. Measurements were carried out along the channel axis throughout the region of large magnetic field strength. The mean ion flow velocity was found to oscillate at the discharge breathing mode frequency of about 21 kHz. By contrast, the ion velocity dispersion appears not to depend on time, which suggests a strong correlation between ionization and acceleration processes. The spatio-temporal behavior of the electric field was computed from experimental data using a Lagrangian description of the ion fluid motion. As expected, the field amplitude varies significantly at 21 kHz. More surprisingly, an electric field front seems to propagate periodically from the exterior toward the interior of the discharge chamber with a speed close to the thermal speed of the Xe atom.

(Some figures in this article are in colour only in the electronic version)

1. Introduction

A Hall effect thruster (HET) is a gridless ion accelerator that offers a versatile fuel-efficient alternative to conventional chemical rocket engines for spacecraft maneuvers that require a large velocity increment [1, 2]. Such an electric propulsive device is currently employed for the positioning of geosynchronous communication satellites. High-power Hall thrusters will soon be used for orbit transfer maneuvers of observation and communication satellites. In addition, large HETs appear as good candidates to be used as the primary propulsion engine for robotic space probes during journeys toward far-off planets and asteroids. A HET is a magnetized low-pressure discharge realized in ring-shaped geometry with crossed electric and magnetic fields [3–5]. A schematic of a HET is depicted in figure 1. The anode is located at the upstream end of a coaxial annular dielectric channel in which the plasma is confined. The magnetic field strength, which is maximum at the channel exhaust, is chosen to be strong enough to trap electrons, but weak enough not to disturb ion trajectories. The supplied gas (usually xenon) is efficiently ionized inside the channel by hot electrons that form the Hall current loop. As the magnetic field considerably slows down the electron diffusion toward the anode, the applied potential concentrates in a restricted area. The resulting axial electric field then accelerates ions out of the channel, which generates thrust. The ion beam is neutralized by a fraction of electrons emitted from the external cathode. When operating near 1.5 kW, a HET ejects ions at 20 km s^{-1} and generates 100 mN of thrust with an overall efficiency of about 50%.

The crossed-field discharge of a Hall thruster is a highly non-stationary medium. It displays numerous types of oscillations, which encompass many kinds of physical phenomena, each with its own length and time scales [4, 6]. Discharge fluctuations, of which the overall frequency range stretches from ~10 kHz up to ~100 MHz, play a major role in ionization, particle diffusion and acceleration processes. Among them, low-frequency oscillations in the 10–30 kHz range, from now on known as breathing oscillations, are especially of interest as they carry the majority of the power [7]. Such oscillations, which find their origin in an ionization instability [8], can merely be interpreted in terms of a

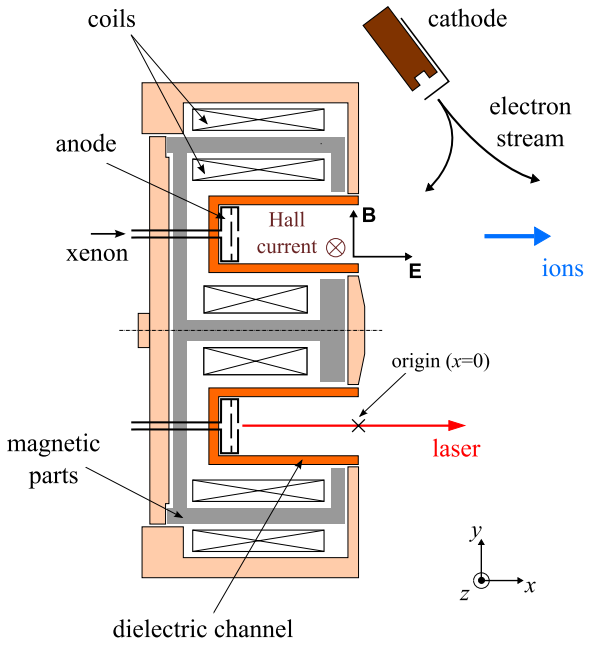

Figure 1. Cross-section view of a Hall effect thruster with measurement reference origin.

prey–predator type mechanism between atoms and ions as shown by various computer simulation works [9–11]. In short, these oscillations originate in a periodic depletion and replenishment of the neutrals near the exhaust of the thruster channel due to the efficient ionization of the gas. The frequency is then linked to the time it takes for atoms to fill in the ionization region. With a xenon atom, thermal speed of about 300 m s^{-1} inside the channel and an ionization region size of ∼20 mm, the frequency is around 15 kHz. Breathing oscillations not only disturb the discharge current but also have a drastic impact on other quantities. The plasma plume shape and the ion beam divergence change during an oscillation cycle of the current, as was shown by means of CCD imaging [12]. Langmuir probe measurements reveal that the electron density and temperature, as well as the plasma potential, oscillate at low frequency in the thruster plume near-field [13, 14]. Changes in time of the aforementioned quantities are most likely connected with a time variation of the potential distribution or, in other words, with the temporal changes in the accelerating electric field. Therefore, it appears of considerable interest to investigate the temporal behavior of the electric field that hides rich and intricate dynamics. Across the acceleration layer, the medium is collisionless, i.e. ion–ion and ion–atom collision events are scarce. As a consequence, using the appropriate numerical method, the electric field can be accurately inferred from the Xe^+ velocity, which then becomes a quantity of prime importance.

Laser induced fluorescence (LIF) spectroscopy in the near infrared is commonly used to measure the time-averaged velocity distribution function (VDF) of Xe^+ ions in the plasma of a HET [15–18]. LIF spectroscopy is a non-intrusive diagnostic tool that enables an accurate determination of the local velocity of atoms and ions along the laser beam direction by measuring the Doppler shift of absorbed photons. The metastable Xe^+ ion VDF is recorded by collecting fluorescence radiation at 541.9 nm after excitation of the $5d\,^2F_{7/2} \rightarrow 6p\,^2D^o_{5/2}$ transition at $\lambda = 834.7233$ nm [18]. A phase sensitive detection method is necessary to capture the fluorescence signal. However, this method offers a poor time resolution. To achieve the measurement of the time-dependent Xe^+ ion VDF in the plasma of a Hall thruster, it is necessary to develop a method able to detect LIF photons with a time resolution around 1 μs. For a HET operating in normal conditions, the number of fluorescence photons observed at 541.9 nm with a continuous laser beam tuned at 834.7233 nm with about 1 mW mm^{-2} power density, is on the order of 10^{-2} μs^{-1}. Under identical experimental conditions, the number of background photons generated by the plasma at 541.9 nm during 1 μs is typically 1, which implies a ratio of 100 between the two signal amplitudes. The optical system must therefore be able (i) to detect a small number of photons hidden in a strong background and (ii) to determine with a high accuracy the exact moment in time the fluorescence photons have been captured. One must therefore turn to a photon-counting technique. The first experimental results that concern the temporal characteristics of the Xe^+ ion VDF within a crossed-field discharge were obtained very recently with a 5 kW-class Hall thruster [19]. The ion axial velocity was indeed found to oscillate at the breathing mode frequency nearby the channel exit plane. Primary observations suggest that ionization and acceleration zones have correlated dynamics through time. Surprisingly, results indicate that the electric field magnitude, which is computed from the mean ion velocity, varies weakly in the course of time, in contrast with numerical simulation outcomes. In the study, LIF measurements were solely performed for three locations along the thruster channel axis: one point far inside the channel and the two others near the exhaust. At that time, it was therefore not possible to come to a clear conclusion about the overall spatio-temporal dynamics of the ion fluid during one breathing oscillation.

The current contribution deals with time-resolved measurements of the Xe^+ ion axial VDF by means of a photon-counting technique in the discharge of the 1.5 kW-class PPS100-ML Hall thruster. The evolution in time of the ion VDF has been recorded at 10 positions equally spaced along the channel centerline, which allows us to precisely reconstruct the temporal behavior of both the ion flow and the accelerating electric field inside and outside the discharge chamber. The time evolution of the ion VDF is examined during a 400 μs time period that follows a 2.5 kHz repetition rate, 10 μs duration break, of the anode current in order to investigate the ion dynamics during forced and free low-frequency discharge oscillations.

2. Diagnostic

2.1. Optical assembly

The optical bench and the collection branch are extensively described in [17, 18]. The laser beam used to excite Xe^+ metastable ions at 834.7 nm is produced by a high-power tunable single-mode external cavity laser diode. The

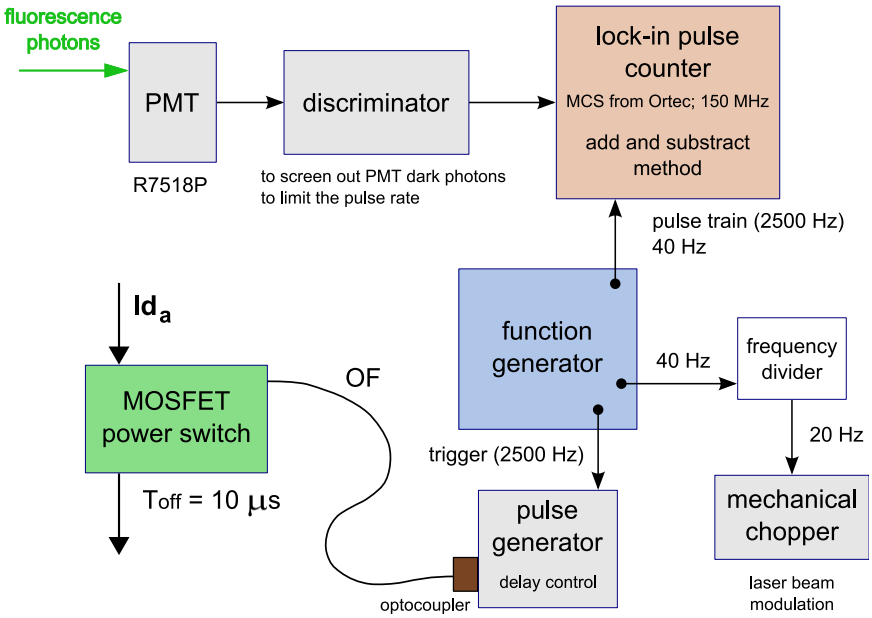

Figure 2. Block diagram of the pulse counting system. The discharge current switch is externally driven by the counter.

wavelength is checked by means of a calibrated wave meter that gives an accuracy of velocity measurement better than 90 m s^{-1}. A high-finesse confocal scanning Fabry–Pérot interferometer is used to check the quality of the laser mode in real time and to detect mode hops. The primary laser beam is modulated by a mechanical chopper before being coupled into a single-mode optical fiber. The fiber output is located behind the thruster. Collimation optics are used to form a narrow beam that passes through a small hole located at the back of the thruster. The laser beam propagates along the channel axis in the direction of the ion flow. The laser power density is maintained to 10 mW mm^{-2} in the detection volume, which warrants a good signal-to-noise ratio and a limited saturation of the observed transition. A collection branch made of a 40 mm focal length lens, which focuses the fluorescence light onto a 200 μm core diameter optical fiber, is mounted onto a travel stage perpendicular to the channel axis. The magnification ratio is 1, meaning that the spatial resolution is 200 μm in the axial direction. A slit was made in the channel outer wall to carry out measurements inside the channel. The fluorescence light is transported by the fiber toward a 20 cm focal length monochromator that isolates the 541.9 nm line from the rest of the spectrum. A photomultiplier tube (PMT) serves as a light detector.

2.2. *Time-resolved photon counting*

The photon-counting technique allows the detection of a very low level signal with an excellent time resolution. When combined with a modulation of the laser light intensity, the counting technique can distinguish between LIF photons and spontaneous emission photons [20]. Here we briefly outline the main characteristics and settings of our system (see [19] for more details). Photons are detected by means of a high gain and low dark noise PMT. A fast amplifier/discriminator module is used to screen out PMT dark current, to limit the pulse rate thereby avoiding saturation of the counter, and to transform any single event—here the arrival of a photon—into a TTL pulse. Pulses are subsequently treated by the pulse counter device, which counts events as a function of time. Our last system is based on a multichannel scaler MCS-pci® from Ortec. A trigger starts the counter, which segments photon count data into sequential time bins. The instrument records the number of photons that arrive in each bin. In order to improve the signal-to-noise ratio considerably, the counter is able to operate in real-time addition–subtraction mode. The laser beam intensity is modulated at $\sim$ 20 Hz by means of a mechanical chopper. Each pulse recorded when the laser is propagating through the plasma is added to the time series. Each pulse recorded when the laser is suspended is subtracted from the time series. A function generator delivers a 2.5 kHz signal that at the same time controls the 10 μs in length discharge current break and triggers the acquisition chain. A block diagram of the counting device is displayed in figure 2. The time resolution, i.e. the width of each bin, was set to 100 ns and 4000 bins were used. The duration of one measurement cycle is therefore 400 μs, corresponding to about eight times the period of low-frequency current oscillations. To obtain a reasonable signal-to-noise ratio, light was accumulated over 1 million cycles. The procedure to obtain the time-dependent ion VDF at a given position consists of accumulating photons in time at a fixed wavelength, i.e. recording the time evolution of a well-defined ion velocity group [19]. About 12 different wavelengths are needed to create a reliable VDF.

2.3. *Experimental conditions*

All measurements were carried out in the PIVOINE-2g test-bench with the 100 mm in outer diameter PPS100-ML Hall effect thruster. The latter was equipped with BN-SiO_2 channel walls. The main thruster parameters were kept unchanged during the experiments: the applied voltage U_d was set to 250 V,

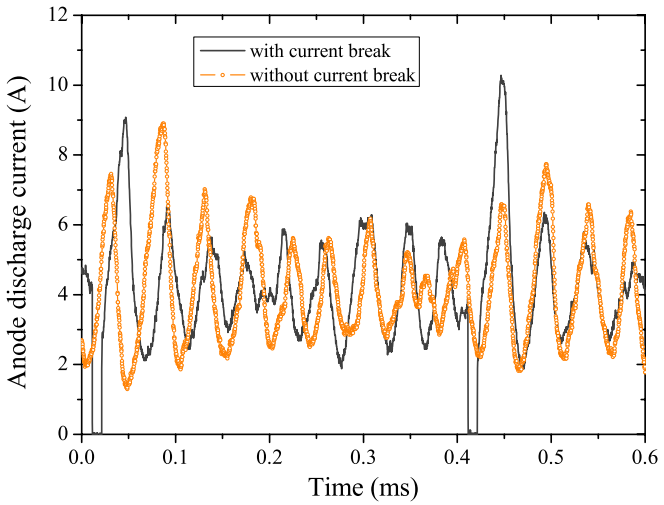

Figure 3. Snapshot of anode discharge current waveforms with (line) and without (circle) a 2.5 kHz power disruption. The current is switched off during 10 μs. The PPS100-ML Hall thruster is fired at 250 V and 4.5 mg s^{-1}.

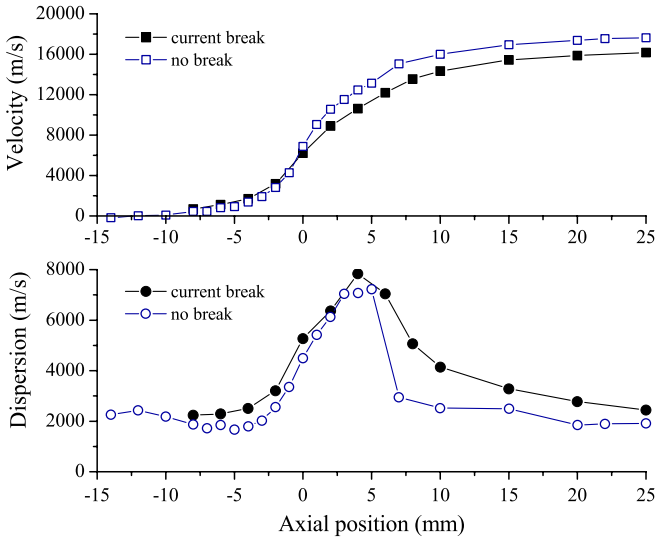

Figure 4. On-axis development of the mean ion velocity (square) and velocity dispersion (circle) with (solid symbol) and without (open symbol) a 10 μs duration current break. The position $x = 0$ corresponds to the channel exit plane.

the anode xenon mass flow rate Φ_a was fixed at 4.5 mg s^{-1} and the current flowing through all coils was set to 5 A. The time-dependent ion VDFs were recorded for 10 equally spaced locations along the channel centerline ranging from $x = -6$ mm to $x = +15$ mm, where the coordinate $x = 0$ refers to the thruster channel exit plane.

As previously mentioned, the ion flow dynamics was investigated after a fast shut-down of the anode discharge current. It was therefore possible to examine the temporal characteristics of the ion VDF during forced and free low-frequency discharge oscillations. The anode current was switched off during 10 μs at 2.5 kHz by way of an optically controlled fast power switch [12]. There was no synchronization between the power cut cycle and the discharge current waveform, i.e. the anode current was switched off randomly at any time with respect to the discharge current natural oscillations. In addition to providing a reference time, current interruption allows us to stabilize the discharge in a quasi-periodic regime, which is crucial for our measurements as data acquisition is a cumulative process over thousands of cycles.

Figure 3 displays the instantaneous waveform of the anode discharge current with and without remote power break. The discharge current vanishes in a few hundred nanoseconds [19]. A current burst always occurs at re-ignition [12]. This forced plasma oscillation originates in the sudden ionization of the large number of propellant atoms accumulated inside the channel when the discharge is turned off. As can be seen in figure 3, apart from the large current peak at re-ignition, the two waveforms are relatively similar, which warrants that trends observed with our approach correspond to a normal plasma behavior. The mean discharge current reaches 4.1 and 4.2 A without and with power disruption, respectively. In contrast, the current standard deviation is clearly influenced by the periodic cut: it is equal to 0.56 A without power disruption against 1.58 A with. The difference is mostly due to cancelation of the current combined with production of a large number of ions when the power is again switched on. The oscillation frequency is found to be ~21 kHz in the two cases, i.e. a time period of about 48 μs.

3. Time-averaged quantities

3.1. Mean velocity and velocity dispersion

The analysis of the steady-state behavior of the Hall discharge is an essential step prior to focusing on the temporal characteristics of the Xe^+ ion velocity. This approach permits us to illustrate the ion fluid properties under our experimental conditions and to clarify the effect of a 10 μs current break on ion velocity and electric field distributions. The time-averaged ion VDF was measured by means of a classical LIF technique employing a lock-in amplifier instead of a pulse counter [18]. The device was operated with a modulation frequency of 1600 Hz and an integration time constant set to 300 ms for all measurement points. The ion VDF is always found to be broader when the current is interrupted. Moreover, the peak of the distribution is shifted toward the low velocity side within the acceleration layer [21]. This is a direct consequence of the production of a large number of standing-still Xe^+ ions at re-ignition. The on-axis development of the mean ion axial velocity is shown in figure 4 for the two conditions. As expected, the final velocity is lower when the current is periodically turned off: 176 40 m s^{-1} against 161 75 m s^{-1}. The accelerating potential experienced by Xe^+ ions is on average 212 V against 178 V. Yet, the size of the acceleration region does not change with the 2.5 kHz external disturbance.

The velocity dispersion p reads as

$$p = 2\sqrt{2Ln(2)} \times \sigma, \qquad (1)$$

where σ is the standard deviation computed from the second order moment of the ion VDF [17]. The quantity p is equal to

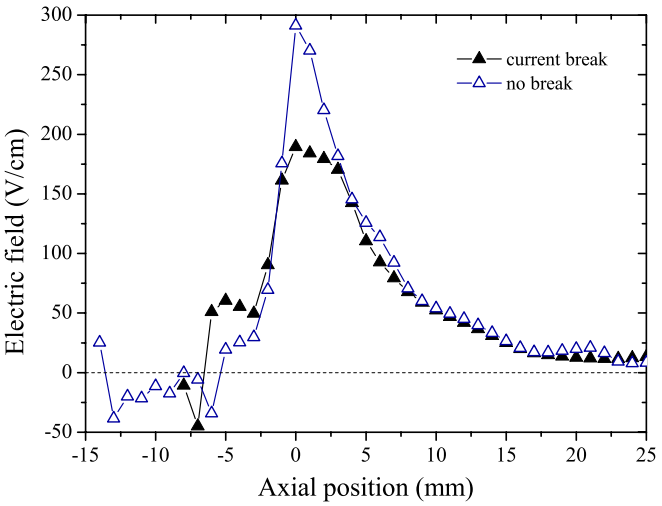

Figure 5. Distribution of the accelerating electric field along the channel axis with (solid triangle) and without (open triangle) a periodic 10 μs current break. Profiles are computed from the high-order moments of the ion velocity distribution function [22].

the full width at half maximum in the case of a Gaussian distribution. The profile of the velocity dispersion along the channel centerline is shown in figure 4. The general shape of the profile does not depend on the thruster operating conditions. As clearly demonstrated in previous studies, the shape reveals the intrinsic overlap between the ionization and acceleration layers [17, 18]. The highest value of p is reached where ionization of the propellant gas ceases. The graph in figure 4 indicates that the velocity dispersion profile is wider when the current is interrupted. The peak stays at $x = -4$ mm, which means the overlap between the two regions is unchanged. The amplitude, however, is affected by the current break: it rises from 7200 m s^{-1} up to 7850 m s^{-1}. Observed facts result from the existence of Xe^+ ions at rest both inside and outside the channel during a short period of time after discharge re-ignition.

3.2. Accelerating electric field

As the ionization and acceleration processes are strongly interrelated in a Hall thruster, the electric field magnitude is in fact underestimated, especially in the region of ionization, when it is calculated from the mean ion velocity [18]. As shown by Pérez-Luna and co-workers, an empirical method based on high-order moments of the ion VDF provides a more accurate value of the electric field [22]. This approach was therefore employed in this study to compute the electric field distribution along the channel axis from measured ion VDF. Resulting curves are plotted in figure 5. The electric field is strongest in the vicinity of the channel exhaust whatever the current waveform. Moreover, a large part of the accelerating field is situated outside the channel. These two properties are ordinary for a Hall thruster discharge [15–18]. They reveal the close link between electron diffusion through the magnetic barrier and ion acceleration process. Nevertheless, as can been observed in figure 5, the electric field magnitude strongly depends on experimental conditions. The amplitude is larger when the discharge current is not periodically cut: 290 V cm^{-1} against 190 V cm^{-1}. As a consequence, performances are inferior with interruptions: the thrust efficiency is only 47% versus 52% under normal conditions. The acceleration region, however, stays roughly unchanged, stretching out from $x = -6$ mm to $x = 20$ mm. In the remainder of the article, we will explore the spatio-temporal variations of the ion axial velocity throughout this region, aiming at a better grasp of the low-frequency behavior of a Hall discharge.

4. Spatio-temporal characteristics of the ion velocity

4.1. Time series of the fluorescence signal

Figure 6 shows several raw fluorescence signal time series for two different positions along the channel axis. Each time series does in fact correspond to the evolution in time of a well-defined ion velocity group. For all traces, the anode current is switched off 6.3 μs after the trigger signal is emitted. At $x = -2$ mm, the steady-state potential drop is weak and ionization still occurs. In contrast, at $x = 8$ mm, the potential drop is large and ionization is stopped. Loss and creation of ion velocity groups when the current is cut then restored was investigated thoroughly in a previous paper [19]. In this work, we mostly consider the oscillatory regime that follows the ion density burst. In figure 6, the ion population that forms a velocity group obviously varies in time, the oscillation amplitude depending both on the ion family and on the location. Neglecting the first oscillation, the ion density mean oscillation frequency is 20.6 kHz, in agreement with the thruster discharge current natural oscillation frequency (see section 2.3). The measured ion density instability results from the competition between ionization of slowly moving neutrals and ejection of fast ions out of the channel [9–11]. Meanwhile, figure 6 reveals another interesting, and relevant, fact: at a fixed position the various fluorescence light time series are not in phase. This is indisputable evidence that the ion velocity oscillates in space too.

The way the ion flow changes over time will be critically examined in the next sections. Before this, it is opportune to establish the validity of our photon-counting measurement technique. This can be achieved by comparing at each measurement location the time-averaged ion VDF obtained by means of a lock-in detector, with the one built from the temporal average of time-varying fluorescence traces. Results are illustrated in figure 7 for $x = -2$ mm and $x = 8$ mm. As can be seen, the temporally averaged ion VDF does not depend on the fluorescence radiation acquisition device. The ion VDFs clearly depart from equilibrium distributions, as illustrated in figure 7. The shape, which depends on the on-axis position, is mainly due to the interrelation between ionization and acceleration layers [18]. Yet, the 10 μs in length periodic current break reinforces the slow wing and shifts the peak of the distribution to the low velocity side [21].

4.2. Contour plot of the VDF

Figure 8 shows contour plots of the time evolution of the Xe^+ ion VDFs for two positions along the thruster channel axis, respectively, $x = -2$ mm and $x = 8$ mm. A contour map is the combination of all fluorescence time series acquired at

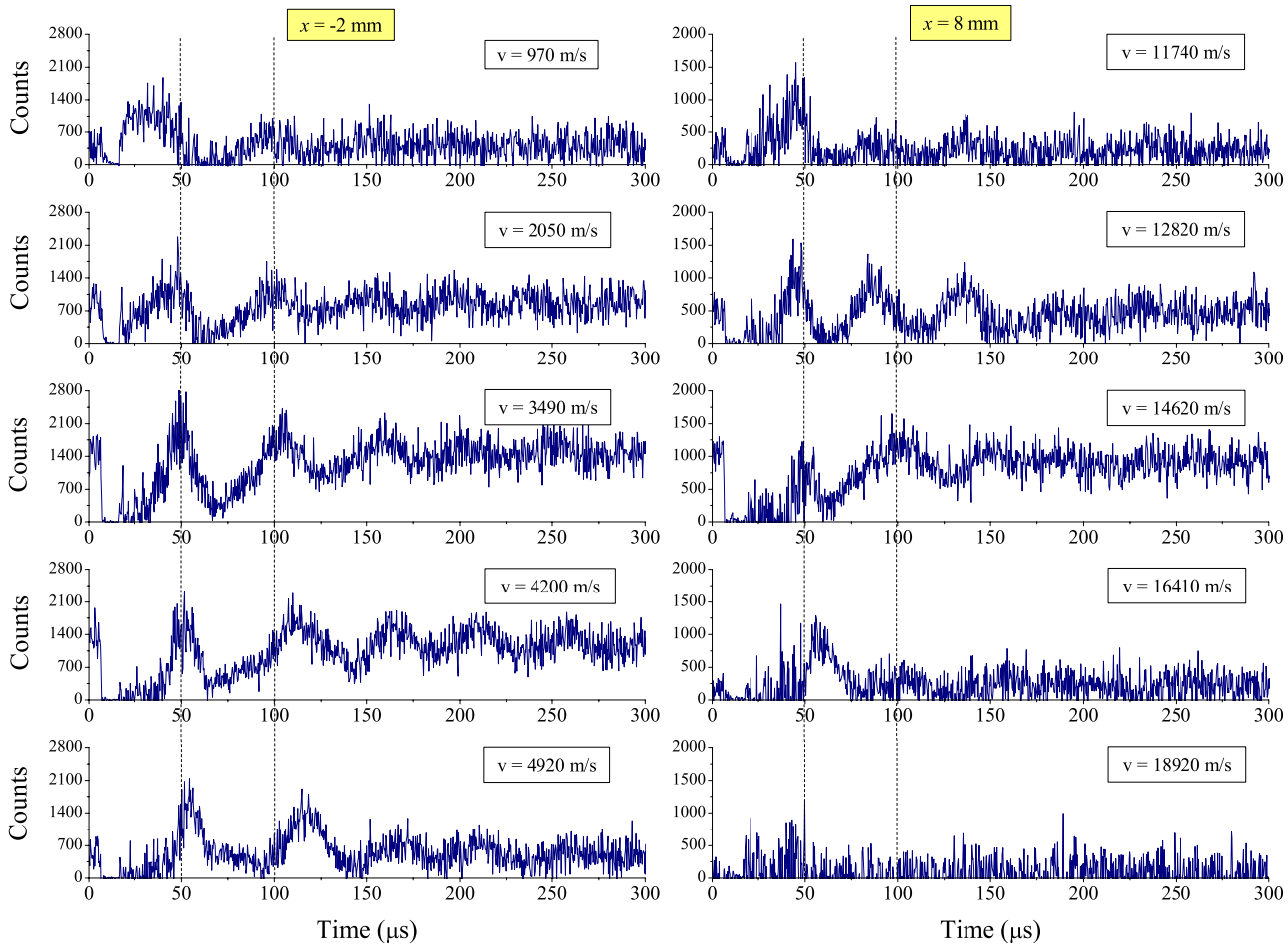

Figure 6. Raw traces of the time evolution of various ion velocity groups at $x = -2$ mm (left) and $x = 8$ mm (right). Lines are drawn to guide the eye.

one position with the photon counter. In figure 8, ions with a relatively low velocity, but above the thermal speed that is around 310 m s^{-1}, are produced everywhere at re-ignition. At $x = -2$ mm, ions flow immediately at about 1000 m s^{-1}. Although electrostatic acceleration is not an instantaneous process, a weak electric field is enough to bring Xe^+ ions to high velocity in a short amount of time. For instance, starting from a null velocity, ions reach 2200 m s^{-1} in 1 μs when experiencing a 30 V cm^{-1} field. This value roughly corresponds to a linear distribution of the 250 V potential applied between the anode and the cathode. Despite being low, the ion velocity after discharge re-ignition is not the same everywhere, being higher outside the channel. It indicates that the electric field is established on a time scale much smaller than the period of the breathing oscillations, with an amplitude larger behind the exit plane. The quick rise in ion velocity right after discharge re-ignition is followed by a gradual increase in the velocity during about 50 μs, until the latter reaches a limit that depends on the location. Subsequently, the ion VDF varies in time with a period of about 50 μs, as can be seen in figure 8, especially during the first free plasma oscillations. This phenomenon indicates that the acceleration potential, and thus the electric field, is likely to oscillate in time with a frequency on the order of the main discharge current oscillation frequency.

4.3. Time evolution of statistical variables

The time evolution of the mean ion axial velocity is shown in the upper graph of figure 9 for the entire area covered in this study. The quantity is computed from the first order moment of the time-dependent ion velocity distribution. The mean velocity is obviously oscillating in time with amplitude variations around 15% behind the channel exhaust. Furthermore, the velocity is in phase opposition with the anode current: the mean velocity goes through a maximum when the current reaches its lowest amplitude. Hybrid fluid/kinetic models also predict low-amplitude periodical variation of the ion velocity with a strong correlation between discharge current waveform and ion velocity temporal behavior [23]. Another interesting fact is the motion of the maximum value toward the interior of the channel in the course of time, see figure 9. The observed oscillations in space and time of the mean ion axial velocity can be solely explained by a back and forth motion of the acceleration layers and/or a change in the electric field magnitude, as already suggested by the analysis of the ion velocity groups' temporal characteristics.

As can be seen in figure 9, the Xe^+ ion axial velocity dispersion—expressed in terms of p parameter, see section 3.1—does not vary much in time but during the high-amplitude oscillation that follows current restart. The

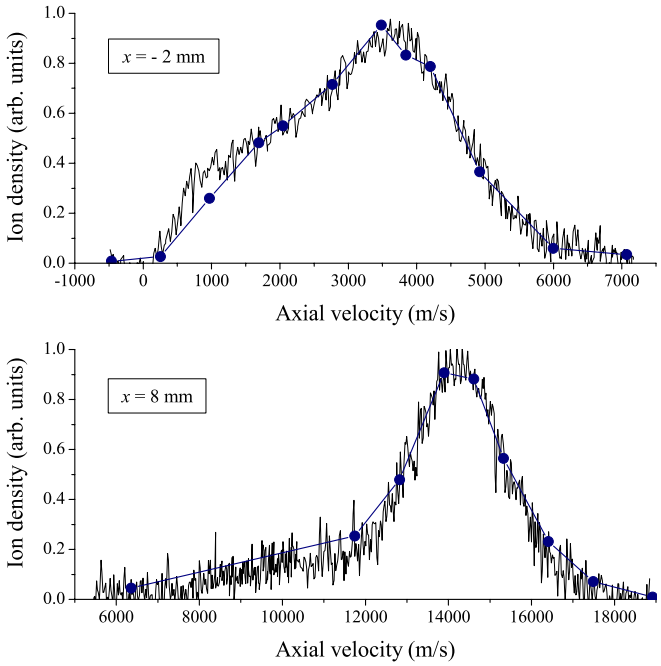

Figure 7. Normalized time-averaged Xe^+ ion velocity distribution function (VDF) at $x = -2$ mm and $x = 8$ mm. The VDF is measured by means of a lock-in detector (line). It is computed from the time-dependent profiles obtained with a photon counter (circle).

dispersion is largest between $x = 3$ mm and $x = 7$ mm, with a maximum instantaneous value close to 9500 m s^{-1}, in good agreement with the time-averaged on-axis profile displayed in figure 4. In a Hall thruster environment the velocity dispersion originates mostly in the spatial overlap between the ionization and the acceleration regions. As the velocity dispersion stays unchanged in the course of time, at least for moderate discharge current fluctuations, whereas the velocity does vary, one can conclude the ionization front and the accelerating potential distribution have correlated dynamics. One possibility would be that the two layers move along together in the axial direction.

5. Low-frequency oscillations of the electric field

Since heavy particle collision events are scarce in the final section of a Hall discharge, ion acceleration is purely electrostatic and the electric field can be extracted from the relationship between the ion kinetic energy and the accelerating potential. However, this approach is only valid either in steady state or when exploring a span of time much longer than the plasma breathing oscillation time period [21]. One must therefore turn toward a more sophisticated way to compute the temporal characteristics of the electric field.

An appropriate method consists of using a Lagrangian description of the ion fluid motion. The electric field can then be computed from the material derivative of the ion velocity, i.e. the derivative taken along a path moving with velocity $\boldsymbol{v}$ [24]. From the equation of motion for unmagnetized ions, the axial component of the electric field E_x reads as

$$E_x = \frac{m}{e}\left(\frac{\partial \bar{v}_x}{\partial t} + \bar{v}_x \cdot \frac{\partial \bar{v}_x}{\partial x}\right), \qquad (2)$$

where m is the ion mass, e is the elementary charge and $\bar{v}_x$ the mean Xe^+ ion axial velocity in the x direction. Note that equation (2) can be obtained from the ion momentum conservation equation for an incompressible fluid assuming a collisionless medium as well as steady and uniform particle density. The evolution of E_x in space and time is given in figure 10. As expected from the time evolution of the mean velocity, the electric field oscillates with a time period of $\sim$50 μs. Disregarding the strong amplitude jump that follows the discharge current ignition, the amplitude change is about 40 V cm^{-1} right behind the channel exit plane ($\approx$20%). The electric field is mostly localized within a region that stretches from $x = -2$ mm to $x = 8$ mm, in agreement with the graph in figure 5. The potential drop that ions undergo at any moment in the vicinity of the channel exhaust can easily be calculated from the $E_x(t, x)$ map. Actually, the potential appears to be independent of time with a value of 155 V in the investigated area. This merely indicates that the region over which the electric field does vary has a limited extent. The potential magnitude is below the one inferred from the final ion velocity. The explanation is twofold. The mean velocity is employed to compute $E(t, x)$, thus the electric field intensity is underestimated inside the channel where ions are created. Moreover, the acceleration layer is not entirely covered in this experiment as measurements stop at $x = 15$ mm. From the contour plot in figure 10, it can be seen that the electric field does not only oscillate through time but also exhibits changes in space. During one oscillation of the discharge current, an electric field front seems to propagate toward the interior of the channel at low velocity. For the first forced oscillation, the front velocity is around 550 m s^{-1}, whereas for all other oscillations the velocity is $\sim$250 m s^{-1}. The velocity is close to the xenon atom thermal speed, which is 310 m s^{-1} under our conditions, assuming that the atom gas is in thermal equilibrium with the channel dielectric walls [25]. Therefore, the electric field, or in other words the acceleration layer, would move with the ionization layer as a direct consequence of the prey–predator process at the origin of the Hall discharge breathing oscillation. This was expected as the ion velocity dispersion stays almost unchanged in time, see section 4.3.

Although experimental results show that near the thruster exit plane an electric field front propagates upstream periodically, the observed phenomenon could be artificially amplified or distorted. Indeed, any momentum source term is taken into account when computing $E(t, x)$, see equation (2). In particular, the impact of ionization and electron pressure is neglected in our approach. Another, more powerful, method was then investigated to account for the main physical mechanisms and to avoid using the mean ion velocity. Following the idea first proposed by Pérez–Luna and co-workers [22], the second approach is based on the one-dimensional time-dependent Boltzmann equation for unmagnetized ions. The equation solely incorporates ion creation; charge-exchange and momentum transfer collision events are disregarded. Starting from this dedicated Boltzmann equation, we demonstrated that $E(t, x)$ can be determined from an expression that contains normalized high-order moments (up to the fourth) of the time-varying ion VDF and their

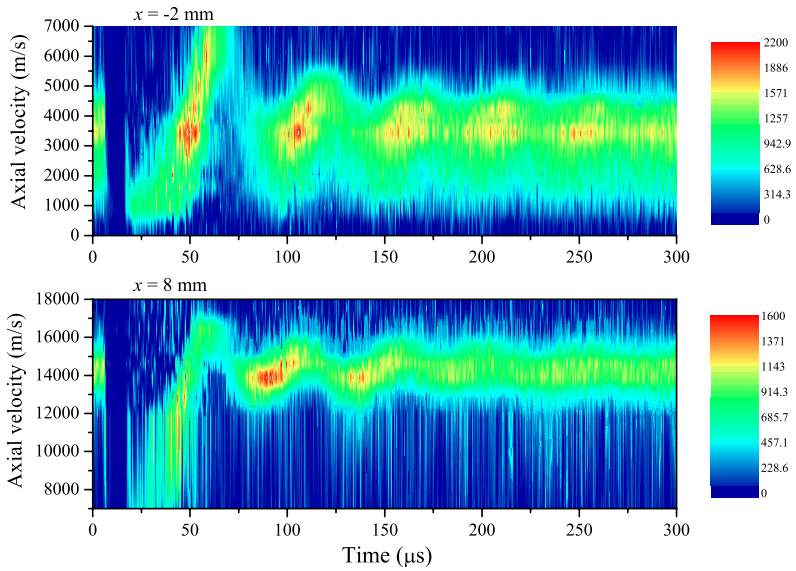

Figure 8. Contour map of the Xe^+ ion axial velocity distribution function as a function of time for two locations along the channel axis. The colorbar indicates the number of counts.

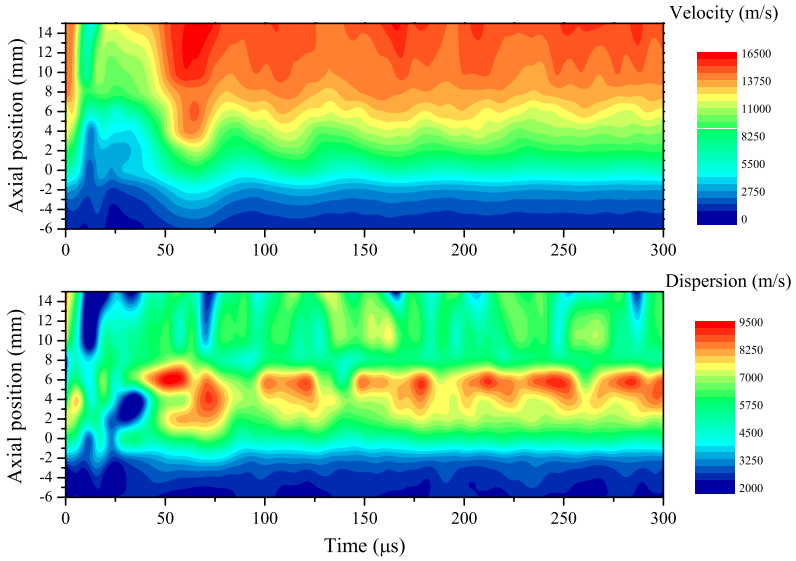

Figure 9. Evolution in space and time of the ion fluid velocity (upper plot) and the velocity dispersion (lower plot).

derivatives [21]. This sophisticated method is, however, extremely noise sensitive. Therefore, due to spreading and amplification of measurement noise during successive calculation steps, no relevant conclusion could so far be drawn from the obtained $E(t, x)$ plot [21]. The influence of ionization on the electric field dynamics in a Hall thruster remains an open question.

6. Conclusion

The time evolution of the Xe^+ ion velocity was examined within the discharge of a PPS100-ML Hall thruster operating at 1 kW by means of laser-induced fluorescence spectroscopy in the near infrared. A pulse-counting detection technique was used to achieve the necessary time resolution in combination with a

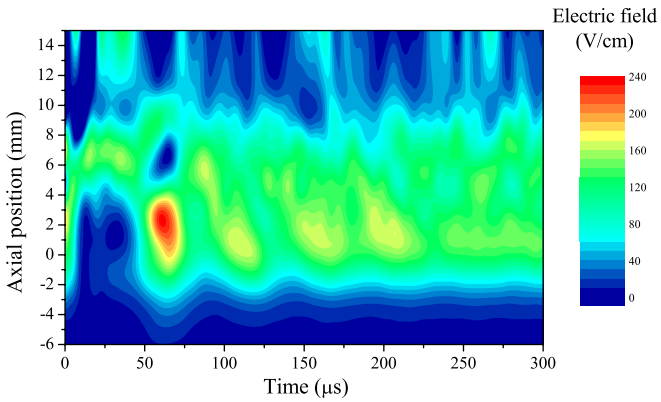

Figure 10. Spatio-temporal characteristics of the axial electric field computed from a Lagrangian description of the ion fluid motion.

periodical short break of the discharge current. The mean ion flow velocity was found to oscillate in the region of the large magnetic field at the breathing mode frequency, which is equal to ∼21 kHz. By contrast, the ion velocity dispersion does not change over time, which implies a strong correlation between ionization and acceleration processes. The spatio-temporal behavior of the electric field was computed from experimental data using a Lagrangian description of the ion fluid motion. As expected, the field amplitude varies significantly at 21 kHz. Another interesting outcome of our treatment is the fact that an electric field front propagates periodically in the x direction from the exterior toward the interior of the discharge chamber with a speed close to the Xe atom thermal speed. Although this property must be confirmed, it indicates the atomic gas temperature is a discharge key parameter.

Other experiments are of course necessary to better grasp the spatio-temporal behavior of the electric field in a crossed-fields Hall discharge. Time-resolved measurements in the y and z directions are of considerable interest since our observations taken along the channel axis are compatible with a low-frequency helical motion of the entire plasma. The investigation of the effect of power level and thruster sizes on the ion velocity time evolution is another important aspect. Finally, a complete understanding of the dynamics of the ion fluid would also require meticulous comparisons between experimental data and computer simulations.

Acknowledgments

The authors wish to acknowledge Dr Nader Sadeghi from the Joseph Fourier University in Grenoble for fruitful discussions. Works were performed in the frame of the joint-program CNRS/CNES/SNECMA/Universities 3161 entitled '*Propulsion par plasma dans l'espace*'. They were also financially supported by the French National Research Agency within the 06-BLAN-0171 TELIOPEH project.

References

[1] Frisbee R H 2003 Advanced space propulsion for the 21st century *J. Propul. Power* **19** 1129
[2] Goebel D M and Katz I 2008 *Fundamentals of Electric Propulsion* (New York: Wiley)
[3] Martinez-Sanchez M and Pollard J E 1998 Spacecraft electric propulsion—an overview *J. Propul. Power* **14** 688
[4] Zhurin V V, Kaufmann H R and Robinson R S 1999 Physics of closed drift thrusters *Plasma Sources Sci. Technol.* **8** R1
[5] Kim V 1998 Main physical features and processes determining the performance of stationary plasma thrusters *J. Propul. Power* **14** 736
[6] Choueiri E Y 2001 Plasma oscillations in Hall thrusters *Phys. Plasmas* **8** 1411
[7] Kurzyna J, Mazouffre S, Lazurenko A, Albarède L, Bonhomme G, Makowski K, Dudeck M and Peradzynski Z 2005 Spectral analysis of Hall effect thruster plasma oscillations based on the Empirical Mode Decomposition *Phys. Plasmas* **12** 123506
[8] Barral S and Ahedo E 2009 Low-frequency model of breathing oscillations in Hall discharges *Phys. Rev.* E **79** 046401
[9] Fife J M, Martínez-Sánchez M and Szabo J 1997 A numerical study of low-frequency discharge oscillations in Hall thrusters *33rd Joint Propulsion Conf. Exhibit (Seattle, WA)* (Washington, DC: AIAA) paper 97-3052
[10] Boeuf J P and Garrigues L 1995 Low frequency oscillations in a stationary plasma thruster *J. Appl. Phys.* **84** 3541
[11] Chable S and Rogier F 2005 Numerical investigation and modeling of stationary plasma thruster low frequency oscillations *Phys. Plasmas* **12** 033504
[12] Vial V, Mazouffre S, Prioul M, Pagnon D and Bouchoule A 2005 CCD images of Hall effect thruster plume dynamics after ultra-fast current ignition *IEEE Trans. Plasma Sci.* **33** 524
[13] Albarède L, Mazouffre S, Bouchoule A and Dudeck M 2006 Low-frequency electron dynamics in the near field of a Hall effect thruster *Phys. Plasmas* **13** 063505
[14] Smith A W and Cappelli M A 2009 Time and space-correlated plasma potential measurements in the near field of a coaxial Hall plasma discharge *Phys. Plasmas* **16** 073504
[15] Hargus W A Jr and Cappelli M A 2001 Laser-induced fluorescence measurements of velocity within a Hall discharge *Appl. Phys.* B **72** 961
[16] Hargus W A Jr and Charles C S 2008 Near-exit plane velocity field of a 200-Watt Hall thruster *J. Propul. Power* **24** 127
[17] Gawron D, Mazouffre S, Sadeghi N and Héron A 2008 Influence of magnetic field and discharge voltage on the acceleration layer features in a Hall effect thruster *Plasma Sources Sci. Technol.* **17** 025001
[18] Mazouffre S, Kulaev V and Pérez-Luna J 2009 Ion diagnostics of a discharge in crossed electric and magnetic fields for electric propulsion *Plasma Sources Sci. Technol.* **18** 034022
[19] Mazouffre S, Gawron D and Sadeghi N 2009 A time-resolved laser-induced fluorescence study on the ion velocity distribution function in a Hall thruster after a fast current disruption *Phys. Plasmas* **16** 043504
[20] Pellissier B and Sadeghi N 1996 Time-resolved pulse counting lock-in detection of laser induced fluorescence in the prescence of a strong background emission *Rev. Sci. Instrum.* **67** 3405
[21] Bourgeois G, Mazouffre S and Sadeghi N 2009 Examination of the temporal characteristics of the electric field in a Hall effet thruster using a photon-counting technique *31st Int. Electric Propulsion Conf. (Ann Arbor, MI)* paper 09-111
[22] Pérez-Luna J, Hagelaar G J M, Garrigues L and Boeuf J P 2009 Method to obtain the electric field and the ionization frequency from laser induced fluorescence measurements *Plasma Sources Sci. Technol.* **18** 034008
[23] Bareilles J, Hagelaar G J M, Garrigues L, Boniface C, Boeuf J P and Gascon N 2004 Critical assessment of a two-dimensional hybrid Hall thruster model: comparisons with experiments *Phys. Plasmas* **11** 3035
[24] Chen F F 1984 *Introduction to Plasma Physics and Controlled Fusion. Vol 1: Plasma Physics* (New York: Plenum)
[25] Mazouffre S, Echegut P and Dudeck M 2007 A calibrated infrared imaging study on the steady state thermal behavior of Hall effect thrusters *Plasma Sources Sci. Technol.* **16** 13